



g-C₃N₄ Modified by *meso*-Tetrahydroxyphenylchlorin for Photocatalytic Hydrogen Evolution Under Visible/Near-Infrared Light

Yanfei Liu¹ and Zhen Ma^{1,2*}

¹ Shanghai Key Laboratory of Atmospheric Particle Pollution and Prevention (LAP³), Department of Environmental Science and Engineering, Fudan University, Shanghai, China, ² Shanghai Institute of Pollution Control and Ecological Security, Shanghai, China

OPEN ACCESS

Edited by:

Shijie Li,
Zhejiang Ocean University, China

Reviewed by:

Fa-tang Li,
Hebei University of Science and
Technology, China
Xiaofeng Shen,
Zhejiang University of Science and
Technology, China

*Correspondence:

Zhen Ma
zhenma@fudan.edu.cn

Specialty section:

This article was submitted to
Catalysis and Photocatalysis,
a section of the journal
Frontiers in Chemistry

Received: 12 September 2020

Accepted: 06 October 2020

Published: 06 November 2020

Citation:

Liu Y and Ma Z (2020) g-C₃N₄
Modified by
meso-Tetrahydroxyphenylchlorin for
Photocatalytic Hydrogen Evolution
Under Visible/Near-Infrared Light.
Front. Chem. 8:605343.
doi: 10.3389/fchem.2020.605343

A new photocatalyst denoted as mTHPC/pCN was prepared by modifying protonated graphitic carbon nitride (pCN) by *meso*-tetrahydroxyphenylchlorin (mTHPC). Relevant samples were characterized via various methods including zeta potential measurements, X-ray diffraction, Fourier transform infrared spectroscopy, X-ray photoelectron spectroscopy, N₂ adsorption–desorption, transmission electron microscopy, ultraviolet-visible–near-infrared spectroscopy, electrochemical impedance spectroscopy, photocurrent response measurements, electron spin resonance spectroscopy, and phosphorescence spectroscopy. Compared with pCN, mTHPC/pCN shows enhanced absorption in the visible and near-infrared regions and thus higher photocatalytic activity in hydrogen evolution. A possible mechanism for mTHPC/pCN is proposed.

Keywords: g-C₃N₄, *meso*-tetrahydroxyphenylchlorin, photocatalytic, hydrogen evolution, visible/near-infrared light

INTRODUCTION

Graphitic carbon nitride (g-C₃N₄) is a new type of photocatalyst with unique physicochemical characteristics (Zheng et al., 2015). The π -conjugated system of g-C₃N₄ allows for the transfer of charge carriers, and a band gap of around 2.7 eV allows it to work under visible (VIS) light (Wang et al., 2009; Ong et al., 2017). In addition, g-C₃N₄ is thermally and chemically stable. It can be prepared by the thermal polycondensation of inexpensive nitrogen-containing carbon-based precursors such as thiourea, melamine, urea, cyanamide, and dicyandiamide without difficulty (Panneri et al., 2017).

However, the low efficiency in VIS light absorption, high recombination rate of photogenerated electrons and holes, low conductivity, and low specific surface areas (SSAs) of g-C₃N₄ may limit its photocatalytic performance (Zou et al., 2016; Mishra et al., 2019). g-C₃N₄ nanorods/nanotubes (Li et al., 2015; Liu et al., 2017), nanasheets (Zhang J. S. et al., 2015; Murugesan et al., 2019), and porous structures (Zeng et al., 2016; Liu M. J. et al., 2019) have been developed. Metal elements (e.g., Ag; Ge et al., 2011, Cu; Fan et al., 2016, Au; Caux et al., 2019, Pt; Zhou et al., 2019) and non-metal elements (e.g., C; Zhao et al., 2015, N; Fang et al., 2015, P; Ran et al., 2015, Br; Lan et al., 2016, O; Wei et al., 2018, S; Xiao et al., 2020) have been doped into g-C₃N₄. In addition, g-C₃N₄-based heterojunctions (e.g., Bi₂O₂CO₃/g-C₃N₄; Wang Z. Y. et al., 2016, CoTiO₃/g-C₃N₄; Ye et al., 2016, Ag₂MoO₄/g-C₃N₄; Zhang and Ma, 2017b, C/g-C₃N₄; Shen et al., 2017,

Ag₆Mo₁₀O₃₃/g-C₃N₄; Zhang and Ma, 2017a, MoS₂/g-C₃N₄; Liu Y. Z. et al., 2018, Bi₃O₄Cl/g-C₃N₄; Che et al., 2018, TiO₂/g-C₃N₄; Tao et al., 2019, WO₃/g-C₃N₄; Fu et al., 2019, CdS/g-C₃N₄; Qiu et al., 2020, ZnO/g-C₃N₄; Gao et al., 2020, Ba₅Nb₄O₁₅/g-C₃N₄; Wang et al., 2020, Co₃(PO₄)₂/g-C₃N₄; Shi et al., 2020, Cs₃Bi₂I₉/g-C₃N₄; Bresolin et al., 2020) have been developed to enhance the photocatalytic performance. However, few studies have aimed at extending the light absorption range of g-C₃N₄ to the near-infrared (NIR) region.

In the total solar spectrum, the ultraviolet (UV) light ($\lambda < 400$ nm), VIS light ($400 < \lambda < 700$ nm), and NIR light ($\lambda > 700$ nm) account for ~5, 43, and 52%, respectively (Li et al., 2016). Therefore, the development of g-C₃N₄-based photocatalysts that can absorb NIR light is important. Photosensitizers are the general term of molecules that can absorb light and transfer energy to other materials. Some researchers modified g-C₃N₄ with photosensitizers such as phthalocyanine (Zhang et al., 2014), a combination of organic dye and zinc phthalocyanine derivative (Zhang X. H. et al., 2015), μ -oxo dimeric iron (III) porphyrin (Wang D. H. et al., 2016), zinc phthalocyanine (Liu Q. W. et al., 2018), mesotetrakis (carboxyphenyl) porphyrins (Da Silva et al., 2018), copper octacarboxyphthalocyanine (Ouedraogo et al., 2018), zinc phthalocyanine derivative (Zeng et al., 2019), multiporphyrin (Yang et al., 2019), zinc (II) 1, 8(11), 15(18), 22(25)-tetrakis (4-carboxylphenoxy) phthalocyanine (α -ZnTcPc) (He et al., 2019), porphyrin (Tian et al., 2019), Chlorin e6 (Ce6) (Liu et al., 2020a), 3,4,9,10-perylenetetracarboxylic acid anhydride (PTCDA) (Yuan et al., 2020), tetra (4-carboxyphenyl) porphyrin iron (III) chloride (FeTcPP) (Zhang et al., 2020), protoporphyrin (Pp) (Liu et al., 2020b), and naphthalimide-porphyrin (Li L. L. et al., 2020). However, more examples in this regard are needed because this is a very interesting topic.

meso-Tetrahydroxyphenylchlorin (mTHPC or temoporfin) is an NIR light-absorbing photosensitizer used for clinical applications and photodynamic therapy (Navarro et al., 2014). In addition, mTHPC is a second-generation photosensitizer that shows some favorable characteristics under NIR light irradiation (Hinger et al., 2016). For example, multiwalled carbon nanotubes were modified with mTHPC for cancer treatment (Marangon et al., 2016). Polymeric micelles were modified with mTHPC for treating cardiovascular diseases (Wennink et al., 2017). Gold nanoparticles were modified with mTHPC for cancer therapeutic (Haimov et al., 2018). Poly(D,L-lactide-co-glycolide) acid nanoparticles were modified with mTHPC for *in vitro* photodynamic therapy (Boeuf-Muraille et al., 2019). However, to the best of our knowledge, g-C₃N₄ was not modified by mTHPC for photocatalysis.

Supplementary Figure 1 shows the chemical structures of mTHPC and bulk graphitic carbon nitride (bCN). mTHPC has many hydroxyl (-OH) groups, and bCN has many -C-N- groups, making the surfaces of both materials negatively charged (**Supplementary Figure 2**) and thus difficult to combine with each other. Herein, protonated graphitic carbon nitride (pCN) was obtained by treating bCN with hydrochloric acid (HCl) solution (Xie et al., 2018). The surface zeta potential of pCN is positively charged (**Supplementary Figure 2**), so the

negatively charged mTHPC may be combined with pCN to yield a composite photocatalyst (**Figure 1**) that can work more efficiently under VIS light and NIR light.

EXPERIMENTAL SECTION

Synthesis of Bulk Graphitic Carbon Nitride (bCN)

bCN was prepared by high-temperature calcination in a muffle furnace. The details are as follows: 12 g melamine was placed in a 50 mL quartz crucible with a lid, and then the quartz crucible was placed in a muffle furnace. The heating rate was set to be 5°C · min⁻¹. The muffle furnace was heated to 550°C, and the temperature was held for 2 h (Cui et al., 2018a). After the muffle furnace was cooled down, the remaining powders (bCN) were collected and ground for further use.

Preparation of pCN

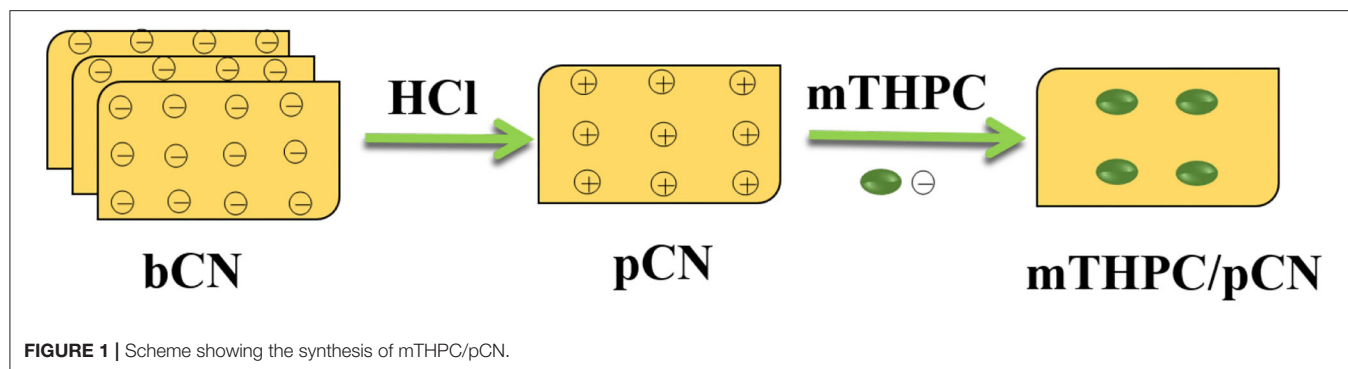
pCN was obtained by treating bCN with HCl solution. The details are as follows: 1 g bCN was placed in 200 mL HCl solution (1 mol · L⁻¹), and the slurry was magnetically stirred at room temperature for 4 h (Cui et al., 2018b). Subsequently, the sediment was collected by high-speed centrifugation, washed with deionized water three times, and dried at 80°C for 12 h. The obtained powders (pCN) were ground for further use.

Preparation of mTHPC/pCN and mTHPC/bCN

mTHPC/pCN was synthesized as follows: 0.5 g pCN was put into 200 mL deionized water, and then 0.05 g mTHPC was added, and the slurry was subjected to magnetic stirring for 2 h at room temperature. Subsequently, the sediment was collected by high-speed centrifugation, washed three times by deionized water, and dried at 80°C for 12 h. The obtained powders (mTHPC/pCN) were collected. In addition, a reference sample denoted as mTHPC/bCN was prepared under the same experimental conditions.

Characterization

The surface zeta potential data were obtained from a Zetasizer Nano ZS device (Malvern Instruments). X-ray diffraction (XRD) data were recorded using a Bruker Advanced D8 (Bruker Corp., Germany) instrument. Fourier transform infrared (FTIR) spectra were recorded by a Nicolet Nexus 470 instrument (Nicolet Instrument Corp., USA). X-ray photoelectron spectra (XPS) were analyzed by an ESCALAB 250 XPS instrument. Nitrogen (N₂) adsorption-desorption were determined by a Tristar 3000 analyzer. Transmission electron microscopy (TEM) images were taken using a JEM-2100F microscope (JEOL, Japan). UV-VIS-NIR absorption spectra were measured by a Cary 5000 spectrophotometer. Electrochemical impedance spectra (EIS) and photocurrent response curves were obtained through a CHI660C electrochemical workstation. Electron spin resonance (ESR) spectra were recorded by a Bruker model A300 spectrometer at room temperature. Phosphorescence spectra were tested on a Hitachi F-4600 spectrometer under an excitation wavelength of 808 nm.



Photocatalytic Hydrogen Evolution

Photocatalytic hydrogen generation experiments were carried out as follows: 10 mg photocatalyst was placed in a 150 mL quartz reactor, 18 mL H₂PtCl₆ solution (0.045 mg · mL⁻¹) was added, and then 2 mL triethanolamine (TEOA) was added. Subsequently, the mixed system was sonicated in an ultrasonic machine for 10 min to allow for the even dispersion of the photocatalyst and then purged with N₂ for 30 min to remove air from the solution and the reactor. During photocatalytic process, the temperature of the photocatalytic reaction was controlled at about 12°C by using circulating cooling water, and a 300-W xenon (Xe) lamp was used as light source. A filter was used to get VIS-NIR light ($\lambda > 420$ nm). Another filter was used to get NIR light ($\lambda > 780$ nm).

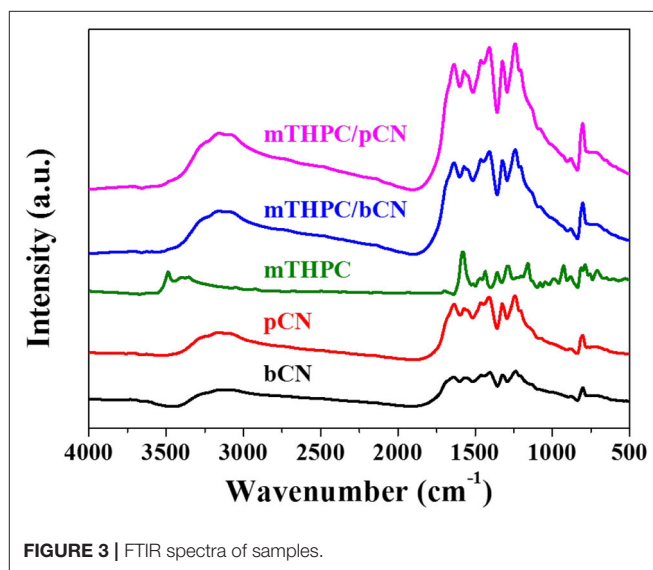
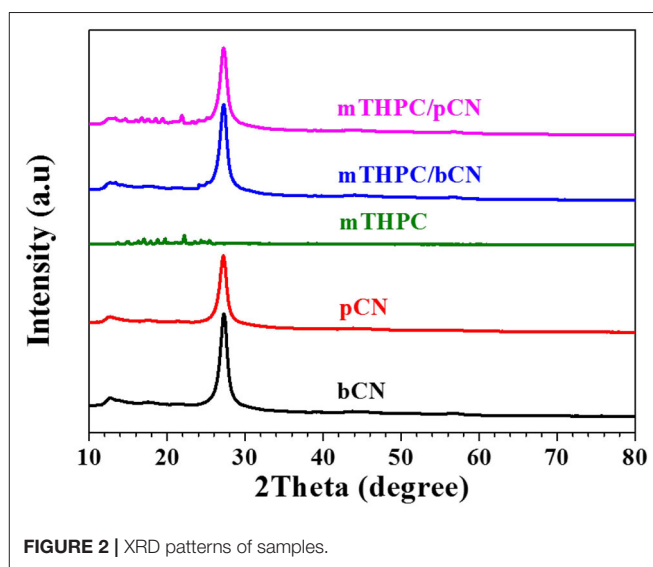
The distance from the light source to the reaction system was 4 cm. The optical power density of the light source was 120 mW · cm⁻² under VIS-NIR light irradiation and 10 mW · cm⁻² under NIR light irradiation. The mixed gas composed of H₂ produced by photocatalysis and N₂ in the quartz reactor was automatically collected and analyzed using a gas chromatograph (GC7600, Tian Mei) every 1 h.

RESULTS AND DISCUSSION

XRD and FTIR Spectra

Figure 2 shows the XRD data. The peak of bCN at 13.4° is attributed to the (100) plane (Inagaki et al., 2019; Qi et al., 2019), and the peak at 27.3° is attributed to the (002) plane (Liu L. et al., 2018; Lee et al., 2019). pCN has the same characteristic peaks as bCN, but the intensity of these peaks decreases to some extent, probably due to the delamination of bCN following the treatment of bCN by HCl solution (Liang et al., 2015; Prabavathi and Muthuraj, 2019). mTHPC shows some weak peaks in the range of 12 to 26° (Yuan et al., 2015a). The peaks of mTHPC are not observed in mTHPC/bCN. However, the peaks of mTHPC can be observed in mTHPC/pCN, indicating the uptake of mTHPC on pCN. In any case, bCN, pCN, mTHPC/bCN, and mTHPC/pCN all show typical g-C₃N₄ patterns.

Figure 3 shows the FTIR spectra of samples. The characteristic peaks of bCN at 800 cm⁻¹ is ascribed to the tri-s-triazine ring units (Zhang et al., 2010; Wang et al., 2019); the broadband peaks at 1,200 to 1,700 nm⁻¹ are attributed to the C-N heterocycles (Liu Q. et al., 2016), and the peaks at 3,000 to 3,500 nm⁻¹ are



attributed to the hydroxyl groups (O-H) and free amino groups (N-H) (Hang et al., 2017; He et al., 2020). pCN has the same

characteristic peaks as bCN, but the intensities of these peaks increase to some extent. mTHPC shows peaks at 700 to 1,700 nm⁻¹, corresponding to (N-H), (C-H), (C=C), and (C=N) (Da Silva et al., 2018). The peaks at 3,250 to 3,600 nm⁻¹ of mTHPC are attributed to the N-H bonds (Yuan et al., 2015b). Although the peaks of mTHPC are not clearly observed in mTHPC/bCN and mTHPC/pCN, all the characteristic peaks of g-C₃N₄ in mTHPC/pCN are the strongest. This may be because mTHPC is loaded on the surface of pCN, which enhances the infrared absorption. A similar trend (enhanced IR absorption) is also seen in the Ce6/pCN (Liu et al., 2020a) and Pp/pGCN (Liu et al., 2020b) systems.

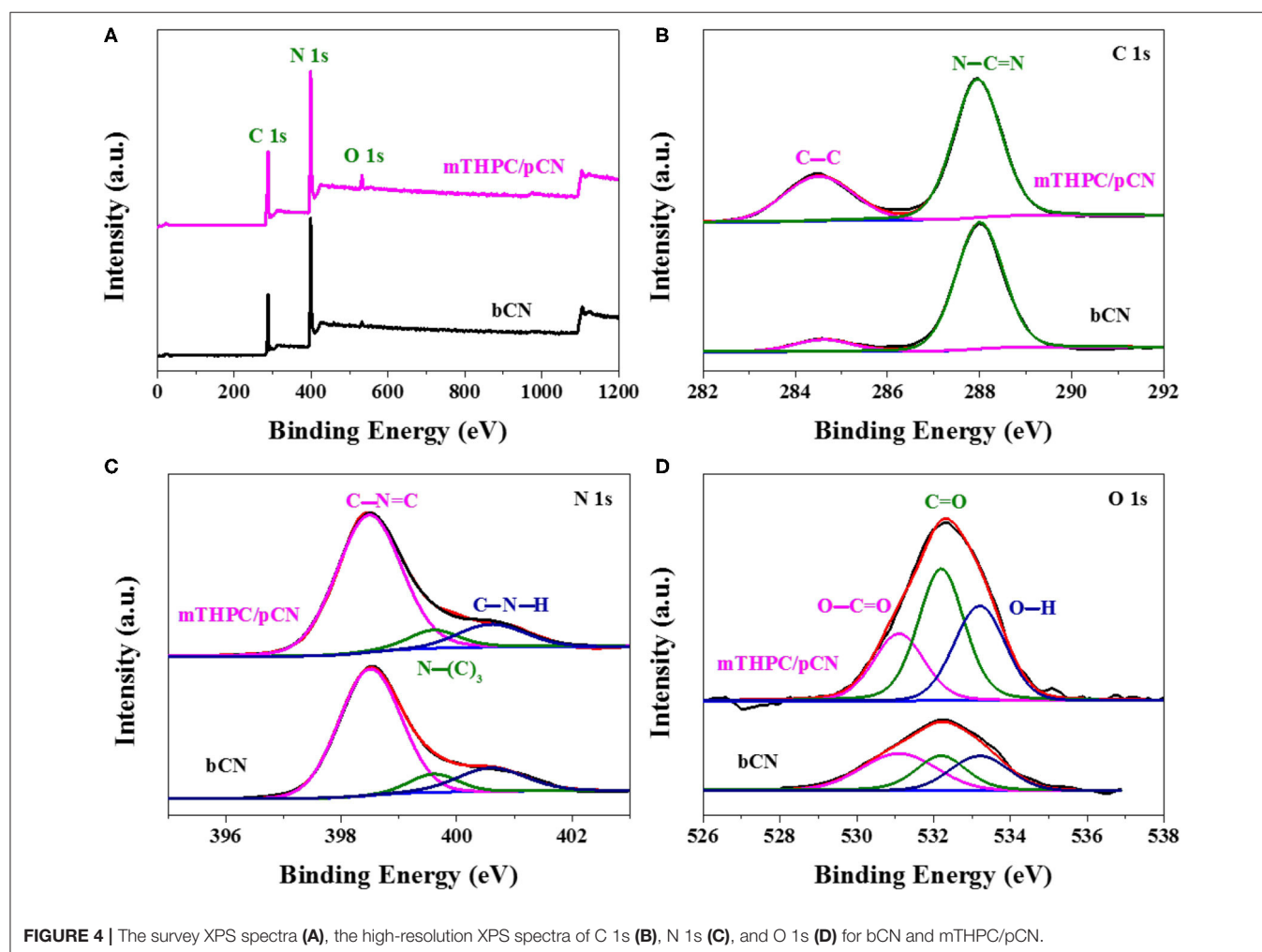
XPS Spectra

Figure 4 shows the XPS spectra of samples. In the survey XPS spectra of bCN and mTHPC/pCN (**Figure 4A**), the peaks of C 1s, N 1s, and O 1s can be obviously observed (Naseri et al., 2017; Zada et al., 2019). **Figure 4B** shows the high-resolution XPS spectra of C 1s. The two peaks at 284.5 and 287.9 eV are assigned to (C-C) and (N-C=N), respectively (Jiang et al., 2017; Liu X. C. et al., 2020). **Figure 4C** shows the high-resolution N 1s XPS spectra. The three peaks at 398.5, 399.6, and 400.6 eV

are assigned to (C-N=C), (N-(C)₃), and (C-N-H), respectively (Sun and Liang, 2017; Sun et al., 2020). **Figure 4D** shows the high-resolution O 1s XPS spectra. The three peaks at 531.1, 532.2, and 533.2 eV are due to O-C=O, C=O, and O-H, respectively (Teng et al., 2017; Zhang et al., 2017). Compared with bCN, the O 1s peaks (especially at 532.2 eV) of mTHPC/pCN are significantly enhanced, probably due to the oxygen-containing group in mTHPC.

N₂ Adsorption-Desorption and TEM Analysis

Supplementary Figure 3 shows the N₂ adsorption-desorption data. The N₂ adsorption and desorption isotherms of samples (**Supplementary Figure 3A**) can be classified as type IV isotherms, signifying the presence of mesopores (2–50 nm) (Qin and Zeng, 2017). The hysteresis loops of samples belong to H3 type, indicating the existence of slit-type mesopores formed by the irregular accumulation of g-C₃N₄ nanosheets (Ding et al., 2017). Compared with bCN, the adsorption volume of pCN appears significantly enhanced and this trend may be due to the nanosheet structure caused by the delamination treatment of



bCN in HCl solution. mTHPC/pCN well maintains the enhanced adsorption volume.

Supplementary Figure 3B shows that the four samples have the wide pore size distribution (2–70 nm), further indicating the presence of mesopores (Qiu et al., 2017). It is worth noting that the pore size distribution curve of pCN has a clear peak at 2 to 5 nm, indicating that the porous structure may be caused by HCl solution, and mTHPC/pCN well maintains the porous structure.

Supplementary Table 1 shows the SSA and pore volume of samples. The SSA and pore volume of bCN are $12.5 \text{ m}^2 \cdot \text{g}^{-1}$ and $0.063 \text{ cm}^3 \cdot \text{g}^{-1}$, respectively. pCN has the largest SSA and pore volume of $40.3 \text{ m}^2 \cdot \text{g}^{-1}$ and $0.163 \text{ cm}^3 \cdot \text{g}^{-1}$, probably due to the delamination treatment of bCN by HCl solution. mTHPC/pCN well maintains a larger SSA and pore volume of $30.8 \text{ m}^2 \cdot \text{g}^{-1}$ and $0.126 \text{ cm}^3 \cdot \text{g}^{-1}$, respectively.

Supplementary Figure 4 shows the TEM images of samples. bCN has the irregularly thick bulk structure (Yu et al., 2017). However, pCN shows the typical two-dimensional nanoflakes and porous structure, consistent with the pore size distribution curve (Mamba and Mishra, 2016). mTHPC/pCN well maintains the ultrathin holey nanosheet structure of pCN.

UV-VIS-NIR Absorption Spectra

Figure 5A shows the UV-VIS-NIR absorption spectra of photocatalysts. bCN and pCN only show obvious absorption capacity in the UV light and VIS light regions (Liu S. Z. et al., 2016) and have almost no absorption capacity in the NIR light region ($\lambda > 780 \text{ nm}$). mTHPC has obvious absorption capacity of the UV light and VIS light and also has obvious absorption capacity in the NIR light range ($\lambda > 780 \text{ nm}$). mTHPC/bCN and

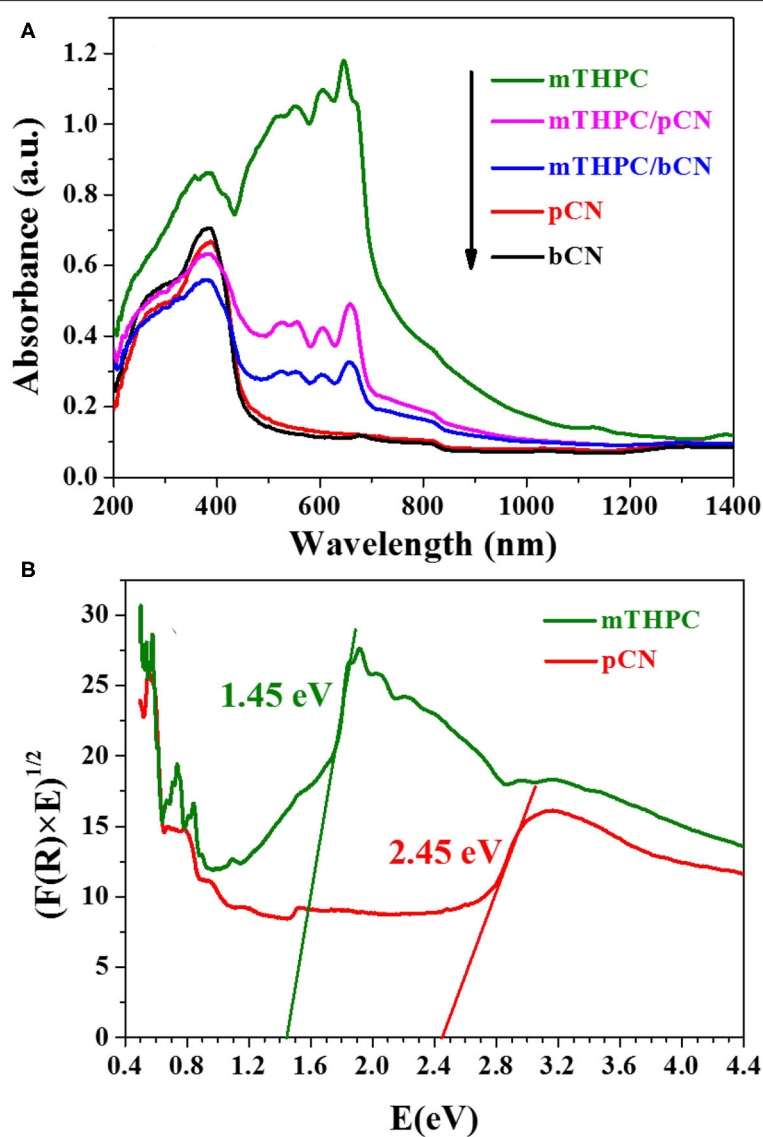


FIGURE 5 | The UV-VIS-NIR absorption spectra of photocatalysts (A) and the calculated energy band gaps (E_g) of mTHPC and pCN (B).

mTHPC/pCN not only maintain the absorption performance of bCN and pCN in the UV light and VIS light range, but also retain the absorption capacity of mTHPC in the NIR light range ($\lambda > 780$ nm) to some extent. Furthermore, the light absorption capacity of mTHPC/pCN is significantly better than that of mTHPC/bCN.

The calculated energy band gaps (E_g) of mTHPC and pCN by the absorption spectra and the equation of $\alpha h\nu = A(h\nu - E_g)^{n/2}$ (Li et al., 2018, 2019) are 1.45 and 2.45 eV in **Figure 5B**, respectively. The α , h , ν , A , E_g , and n stand for the absorption coefficient, the Planck's constant, the light frequency, the proportionality constant, the energy band gap, and $n = 1$ for a direct band gap transition, respectively (Adhikari et al., 2017).

Photocatalytic Hydrogen Evolution

Photocatalytic hydrogen generation was performed under a 300-W xenon (Xe) lamp as the light source. **Figure 6A** shows the photocatalytic hydrogen production performance of samples under VIS-NIR light irradiation. A filter was used to get VIS-NIR light source ($\lambda > 420$ nm), 3 wt.% Pt was used as the co-catalyst, and TEOA was used as the sacrificial reagent. bCN and mTHPC show low hydrogen production performance; the average hydrogen evolution rates (HERs) are 120.6 and 87.4 $\mu\text{mol} \cdot \text{h}^{-1} \cdot \text{g}^{-1}$, respectively.

The average HER of pCN and mTHPC/bCN are 266.0 and 605.8 $\mu\text{mol} \cdot \text{h}^{-1} \cdot \text{g}^{-1}$, respectively. mTHPC/pCN shows the highest average HER of $1,041.4$ $\mu\text{mol} \cdot \text{h}^{-1} \cdot \text{g}^{-1}$, somewhat lower than the average HER obtained by Ce6/pCN ($1,275.6$ $\mu\text{mol} \cdot \text{h}^{-1} \cdot \text{g}^{-1}$) (Liu et al., 2020a) and Pp/pGCN ($1,153.8$ $\mu\text{mol} \cdot \text{h}^{-1} \cdot \text{g}^{-1}$) (Liu et al., 2020b). Furthermore, mTHPC/pCN has good cycle stability under VIS-NIR irradiation in **Figure 6B**. The XRD patterns of the fresh mTHPC/pCN and the used mTHPC/pCN are shown in **Supplementary Figure 5**. Compared with the fresh mTHPC/pCN, the peak intensities of the used mTHPC/pCN decrease to some extent, and the used mTHPC/pCN well maintains the crystal structure of the fresh mTHPC/pCN.

Figure 7A shows the photocatalytic hydrogen production activity of samples under NIR light irradiation. A filter was used to get NIR light source ($\lambda > 780$ nm), Pt was used as the cocatalyst, and TEOA was used as the sacrificial reagent. bCN and pCN show trace amounts of hydrogen production, while mTHPC shows the low average HER of 25.1 $\mu\text{mol} \cdot \text{h}^{-1} \cdot \text{g}^{-1}$.

The average HER of mTHPC/bCN is 59.3 $\mu\text{mol} \cdot \text{h}^{-1} \cdot \text{g}^{-1}$. mTHPC/pCN shows the highest average HER of 78.8 $\mu\text{mol} \cdot \text{h}^{-1} \cdot \text{g}^{-1}$, lower than the rate obtained by Ce6/pCN (312.6 $\mu\text{mol} \cdot \text{h}^{-1} \cdot \text{g}^{-1}$) (Liu et al., 2020a) and Pp/pGCN (307.8 $\mu\text{mol} \cdot \text{h}^{-1} \cdot \text{g}^{-1}$) (Liu et al., 2020b). This may be because the UV-VIS-NIR absorption capacity of mTHPC is lower than that of Ce6 and Pp (**Supplementary Figure 6**). In addition, mTHPC/pCN has good cycle stability under NIR irradiation in **Figure 7B**.

EIS, Photocurrent Response Curves, ESR, and Phosphorescence Spectra

Figure 8 shows the EIS comparison of bCN and mTHPC/pCN. The arc size in the high-frequency region of the Nyquist diagram

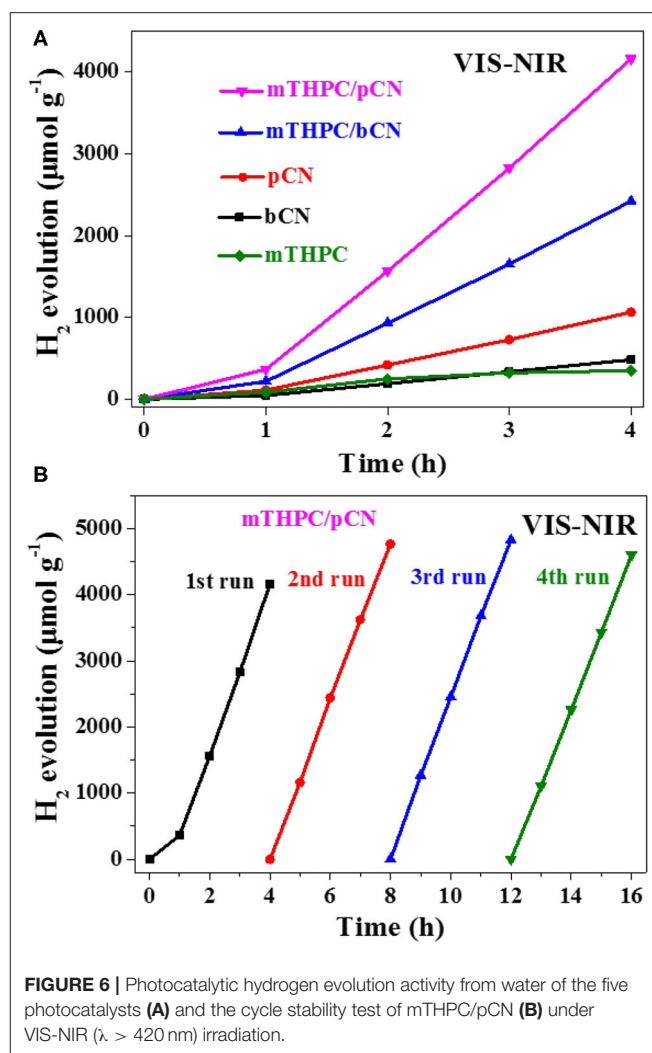


FIGURE 6 | Photocatalytic hydrogen evolution activity from water of the five photocatalysts (A) and the cycle stability test of mTHPC/pCN (B) under VIS-NIR ($\lambda > 420$ nm) irradiation.

is consistent with the electron transfer restriction mechanism, and the arc diameter is equal to the resistance of the electron transfer (She et al., 2016; Li S. J. et al., 2020). Obviously, the arc radius of mTHPC/pCN is significantly smaller than bCN, indicating that mTHPC/pCN can significantly retard the recombination of photogenerated electrons and holes and accelerate electron transfer (Li et al., 2017).

Figure 9 shows the transient photocurrent response curves comparison of bCN and mTHPC/pCN under VIS-NIR ($\lambda > 420$ nm) irradiation. When turning on the light source, the photocurrents of the two samples rise immediately (Shen et al., 2020a). Conversely, when turning off the light source, the photocurrents drop quickly (Luo et al., 2018; Li et al., 2021). The pattern can be repeated, indicating that photogenerated electrons can be transferred to the contact interface through the sample under light irradiation (Tian et al., 2017; Shen et al., 2020b). Further observation found that the photocurrent value of mTHPC/pCN is higher than bCN, indicating that the charge separation efficiency of mTHPC/pCN has significantly enhanced (An et al., 2017).

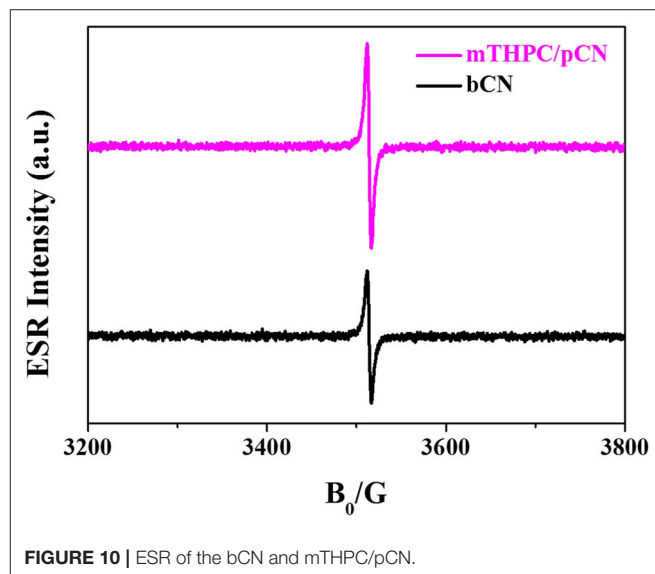
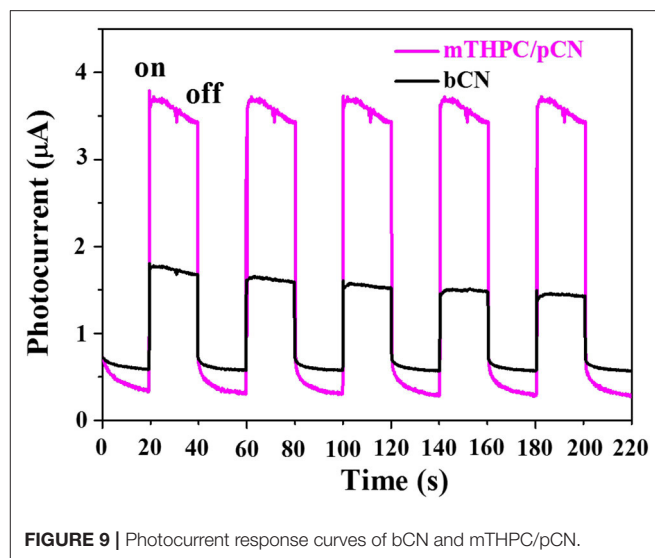
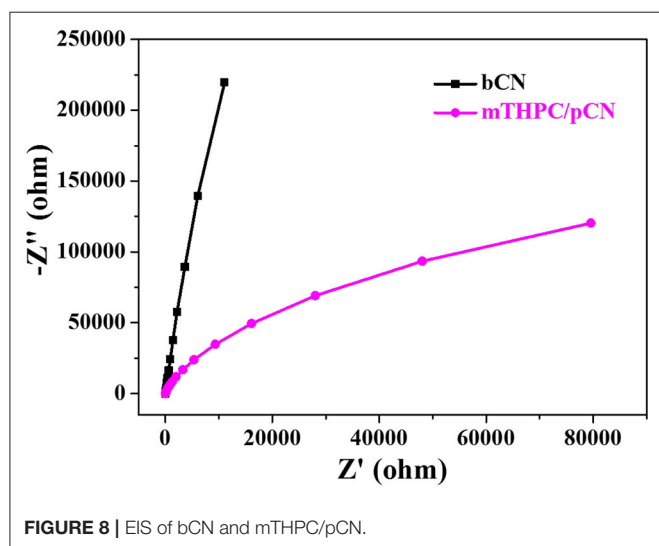
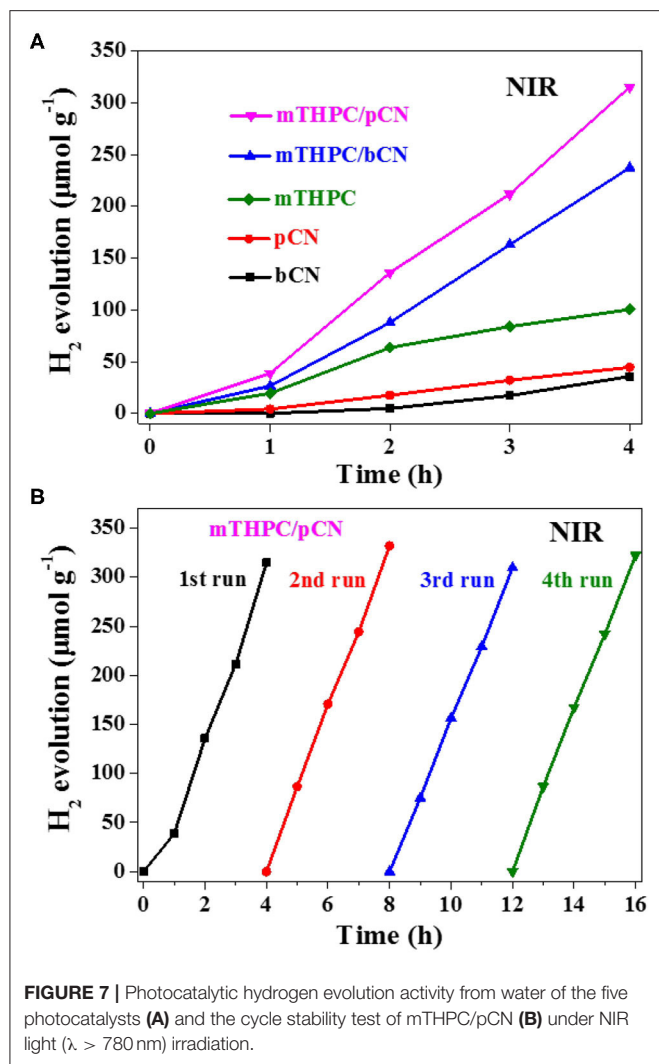


Figure 10 exhibits the ESR characterization of bCN and mTHPC/pCN under NIR light ($\lambda > 780$ nm) at room temperature. bCN and mTHPC/pCN both exhibit one single Lorentz line ($g = 2.0034$) from 3,200 to 3,800 G magnetic field (Liu G. et al., 2019; Jia et al., 2020). However, compared with bCN, the ESR intensity of mTHPC/pCN is much stronger, indicating that the concentration of unpaired electrons is much higher.

The phosphorescence spectra of mTHPC and mTHPC/pCN were tested at an excitation wavelength of 808 nm at room temperature in **Figure 11**. Obviously, the emission wavelength of mTHPC is in the range of VIS light (400–600 nm), indicating that the mTHPC has obvious up-conversion behavior (Wang et al., 2018). Compared with mTHPC, the emission peak intensity of mTHPC/pCN is significantly decreased, indicating the energy transfer from mTHPC to pCN.

Photocatalytic Mechanism

The energy band gaps (E_g) of mTHPC and pCN are 1.45 and 2.45 eV in **Figure 5B**, respectively. The XPS valence band (VB) top position of mTHPC and pCN are 0.62 and 1.29 V in **Supplementary Figure 7**, respectively. Thus, contrasting to the standard hydrogen electrode potential, the

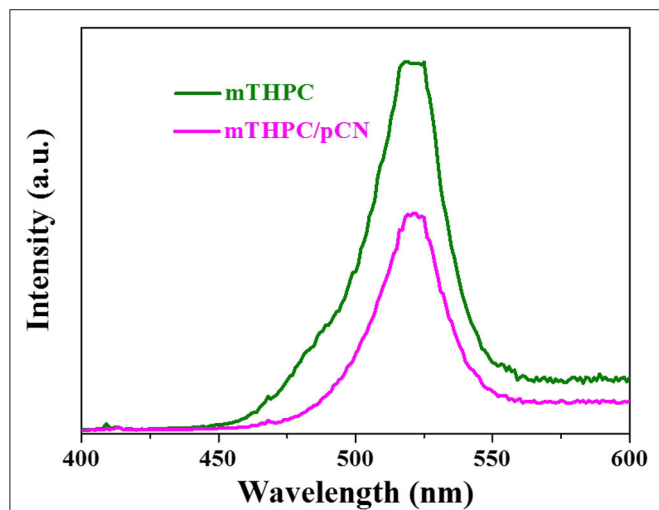


FIGURE 11 | The photoluminescence spectra of mTHPC and mTHPC/pCN.

conduction bands (CBs) of mTHPC and pCN are -0.83 and -1.16 V, respectively.

A possible mechanism for mTHPC/pCN is proposed in **Figure 12**. When mTHPC/pCN is irradiated under VIS light, pCN is excited to generate electrons (e^-) on CB and holes (h^+) on VB. Because the CB edge potential of pCN (-1.16 V) is more negative than that of mTHPC (-0.83 V), the e^- on pCN could transfer to the CB of mTHPC. Pt was used as the cocatalyst (**Figure 13** and **Supplementary Figure 8**) obtained from the Pt precursor ($H_2PtCl_6 \cdot 6H_2O$) by the *in situ* photoreduction (Sui et al., 2013; Pan et al., 2017). Pt nanoparticles may slightly enhance absorption intensity in NIR region (**Supplementary Figure 9**) due to the light scattering phenomenon of Pt (Shiraishi et al., 2014; Chen et al., 2020). Pt can quickly transfer e^- which can reduce H^+ to H_2 (Xing et al., 2014; Zhou et al., 2019). Indeed, the photocatalytic hydrogen evolution performance is significantly enhanced (**Supplementary Figure 10**). In addition, because the VB of pCN (1.29 V) is more positive than that of mTHPC (0.62 V), the h^+ on pCN could transfer to the VB of mTHPC. As the sacrificial agent, TEOA can quickly transfer h^+ and be used as TEOA to TEOA $^+$ (Xing et al., 2014; Zhou et al., 2019).

When mTHPC/pCN is irradiated under NIR light, mTHPC has an up-conversion behavior (**Figure 11**); i.e., the irradiation of mTHPC under NIR light can generate VIS light for pCN to work. Actually, the ESR characterization showed the concentration of unpaired electrons is much higher

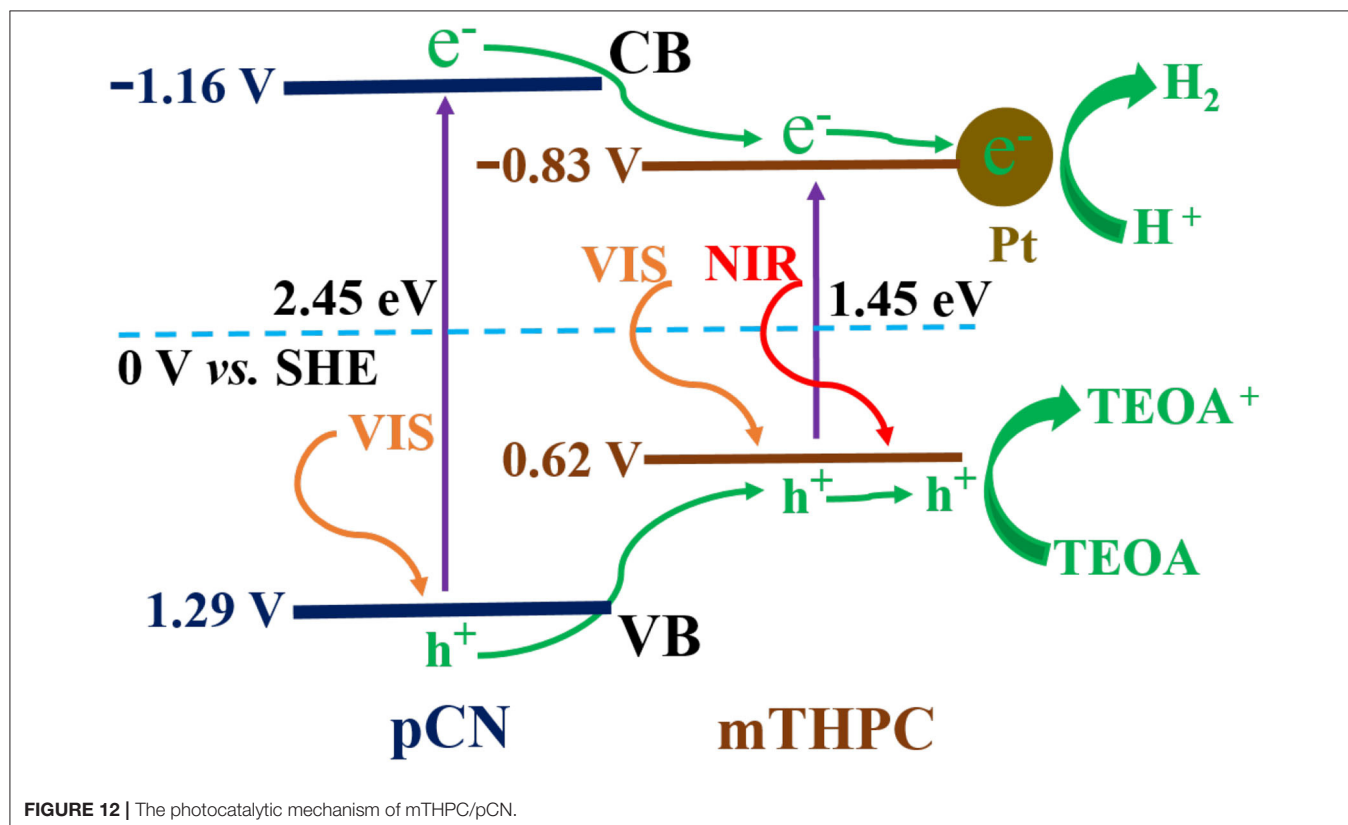


FIGURE 12 | The photocatalytic mechanism of mTHPC/pCN.

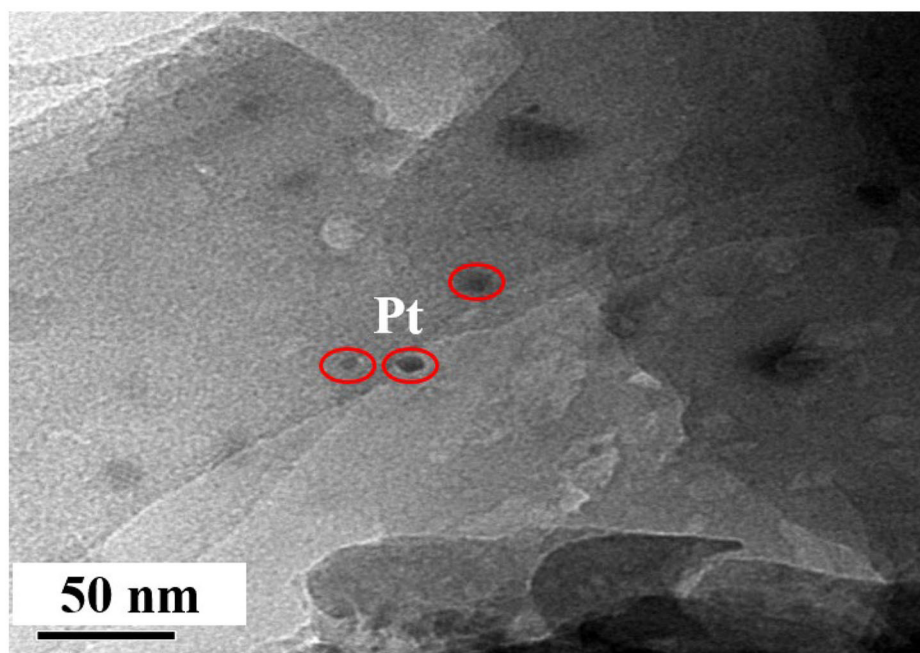


FIGURE 13 | The TEM image of mTHPC/pCN collected after conducting photocatalytic reaction for one time.

in mTHPC/pCN than bCN under NIR light irradiation (Figure 10). In addition, although under NIR light irradiation only, mTHPC/pCN still works because of its NIR absorption capacity (Figure 5A) and the up-conversion behavior of mTHPC (Figure 11).

CONCLUSIONS

mTHPC/pCN prepared by positively charged pCN was modified by negatively charged mTHPC for the first time. mTHPC/pCN can allow for efficient charge separation and transfer and retard the recombination of photogenerated electrons and holes. In addition, mTHPC/pCN has a wide range of VIS light and NIR light absorption capabilities and thus the enhanced photocatalytic hydrogen evolution performance and good stability. The current results show that using a photosensitizer can enhance the light absorption intensity of the VIS light-driven g-C₃N₄ system and expand the absorption and utilization of the solar spectrum range. This work provides some new insights and directions for the

realization of photocatalytic hydrogen evolution under VIS/NIR light region.

DATA AVAILABILITY STATEMENT

The raw data supporting the conclusions of this article will be made available by the authors, without undue reservation.

AUTHOR CONTRIBUTIONS

YL came up with the idea, designed the experiments, analyzed the data, and wrote the paper. ZM guided the research and revised the paper. Both authors contributed to the article and approved the submitted version.

SUPPLEMENTARY MATERIAL

The Supplementary Material for this article can be found online at: <https://www.frontiersin.org/articles/10.3389/fchem.2020.605343/full#supplementary-material>

REFERENCES

- Adhikari, S. P., Hood, Z. D., Wang, H., Peng, R., Krall, A., Li, H., et al. (2017). Enhanced visible light photocatalytic water reduction from a g-C₃N₄/SrTa₂O₆ heterojunction. *Appl. Catal. B Environ.* 217, 448–458. doi: 10.1016/j.apcatb.2017.05.092
- An, X. H., Cao, Y. Q., Liu, Q., Chen, L., Lin, Z. G., Zhou, Y. G., et al. (2017). Graphitic carbon/carbon nitride hybrid as metal-free photocatalyst for enhancing hydrogen evolution. *Appl. Catal. A Gen.* 546, 30–35. doi: 10.1016/j.apcata.2017.07.046
- Boeuf-Muraille, G., Rigaux, G., Callewaert, M., Zambrano, N., Van Gulick, L., Roullin, V. G., et al. (2019). Evaluation of mTHPC-loaded PLGA nanoparticles for in vitro photodynamic therapy on C6 glioma cell line. *Photodiagn. Photodyn. Ther.* 25, 448–455. doi: 10.1016/j.pdpdt.2019.01.026
- Bresolin, B. M., Sgarbossa, P., Bahnemann, D. W., and Sillanpää, M. (2020). Cs₃Bi₂I₉/g-C₃N₄ as a new binary photocatalyst for efficient

- visible-light photocatalytic processes. *Sep. Purif. Technol.* 251:117320. doi: 10.1016/j.seppur.2020.117320
- Caux, M., Menard, H., AlSalik, Y. M., Irvine, J. T. S., and Idriss, H. (2019). Photocatalytic hydrogen production over Au/g-C₃N₄: effect of gold particle dispersion and morphology. *Phys. Chem. Chem. Phys.* 21, 15974–15987. doi: 10.1039/C9CP02241D
- Che, H. N., Che, G. B., Dong, H. J., Hu, W., Hu, H., Liu, C. B., et al. (2018). Fabrication of Z-scheme Bi₂O₄Cl/g-C₃N₄ 2D/2D heterojunctions with enhanced interfacial charge separation and photocatalytic degradation various organic pollutants activity. *Appl. Surf. Sci.* 55, 705–716. doi: 10.1016/j.apsusc.2018.06.038
- Chen, Y. J., Ji, S. F., Sun, W. M., Lei, Y. P., Wang, Q. C., Li, A., et al. (2020). Engineering the atomic interface with single Platinum atoms for enhanced photocatalytic hydrogen production. *Angew Chem. Int. Ed.* 59, 1295–1301. doi: 10.1002/anie.201912439
- Cui, L. F., Liu, Y. F., Fang, X. Y., Yin, C. C., Li, S. S., Sun, D., et al. (2018a). Scalable and clean exfoliation of graphitic carbon nitride in NaClO solution: enriched surface active sites for enhanced photocatalytic H₂ evolution. *Green Chem.* 20, 1354–1361. doi: 10.1039/C7GC03704J
- Cui, L. F., Liu, Y. F., Wang, Y. T., Fang, X. Y., Yin, C. C., Kang, S. F., et al. (2018b). Constructing ultrathin g-C₃N₄ nanosheets with hierarchical pores by NaClO induced wet etching for efficient photocatalytic Cr(VI) detoxification under visible light irradiation. *Diam. Relat. Mater.* 88, 51–59. doi: 10.1016/j.diamond.2018.06.016
- Da Silva, E. S., Moura, N. M. M., Neves, M. G. P. M. S., Coutinho, A., Prieto, M., Silva, C. G., et al. (2018). Novel hybrids of graphitic carbon nitride sensitized with free-base meso-tetrakis(carboxyphenyl) porphyrins for efficient visible light photocatalytic hydrogen production. *Appl. Catal. B Environ.* 221, 56–69. doi: 10.1016/j.apcatb.2017.08.079
- Ding, F., Yang, D., Tong, Z. W., Nan, Y. H., Wang, Y. J., Zou, X. Y., et al. (2017). Graphitic carbon nitride-based nanocomposites as visible-light driven photocatalysts for environmental purification. *Environ. Sci. Nano* 4, 1455–1469. doi: 10.1039/C7EN00255F
- Fan, M. S., Song, C. J., Chen, T. J., Yan, X., Xu, D. B., Gu, W., et al. (2016). Visible-light-driven high photocatalytic activities of Cu/g-C₃N₄ photocatalysts for hydrogen production. *RSC Adv.* 6, 34633–34640. doi: 10.1039/C5RA27755H
- Fang, J. W., Fan, H. Q., Li, M. M., and Long, C. Nitrogen self-doped graphitic carbon nitride as efficient visible light photocatalyst for hydrogen evolution. *J. Mater. Chem. A.* (2015) 3, 13819–13826. doi: 10.1039/C5TA02257F
- Fu, J. W., Xu, Q. L., Low, J. X., Jiang, C. J., and Yu, J. G. (2019). Ultrathin 2D/2D WO₃/g-C₃N₄ step-scheme H₂ production photocatalyst. *Appl. Catal. B Environ.* 243, 556–565. doi: 10.1016/j.apcatb.2018.11.011
- Gao, X. X., Yang, B. Z., Yao, W. Q., Wang, Y. J., Zong, R. L., and Wang, J., et al. (2020). Enhanced photocatalytic activity of ZnO/g-C₃N₄ composites by regulating stacked thickness of g-C₃N₄ nanosheets. *Environ. Pollut.* 257:113577. doi: 10.1016/j.envpol.2019.113577
- Ge, L., Han, C. C., Liu, J., and Li, Y. F. (2011). Enhanced visible light photocatalytic activity of novel polymeric g-C₃N₄ loaded with Ag nanoparticles. *Appl. Catal. A Gen.* 409, 215–222. doi: 10.1016/j.apcata.2011.10.006
- Haimov, E., Weitman, H., Polani, S., Schori, H., Zitoun, D., and Shefi, O. (2018). meso-Tetrahydroxyphenylchlorin-conjugated gold nanoparticles as a tool to improve photodynamic therapy. *ACS Appl. Mater. Inter.* 10, 2319–2327. doi: 10.1021/acsami.7b16455
- Hang, N. T., Zhang, S. L., and Yang, W. (2017). Efficient exfoliation of g-C₃N₄ and NO₂ sensing behavior of graphene/g-C₃N₄ nanocomposite. *Sensor Actuat. B Chem.* 248, 940–948. doi: 10.1016/j.snb.2017.01.199
- He, R. F., Liang, H. O., Li, C. P., and Bai, J. (2020). Enhanced photocatalytic hydrogen production over Co₃O₄@g-C₃N₄ p-n junction adhering on one-dimensional carbon fiber. *Colloid. Surf. A* 586:124200. doi: 10.1016/j.colsurfa.2019.124200
- He, Y. Q., Huang, Z. R., Ma, Z. Y., Yao, B. H., Liu, H. Y., Hu, L. L., et al. (2019). Highly efficient photocatalytic performance and mechanism of α-ZnTePc/g-C₃N₄ composites for methylene blue and tetracycline degradation under visible light irradiation. *Appl. Surf. Sci.* 498:143834. doi: 10.1016/j.apsusc.2019.143834
- Hinger, D., Navarro, F., Kach, A., Thomann, J. S., Mittler, F., Couffin, A. C., et al. (2016). Photoinduced effects of m-tetrahydroxyphenylchlorin loaded lipid nanoemulsions on multicellular tumor spheroids. *J. Nanobiotechnol.* 14, 68–81. doi: 10.1186/s12951-016-0221-x
- Inagaki, M., Tsumura, T., Kinumoto, T., and Toyoda, M. (2019). Graphitic carbon nitrides (g-C₃N₄) with comparative discussion to carbon materials. *Carbon* 141, 580–607. doi: 10.1016/j.carbon.2018.09.082
- Jia, J., Sun, W. J., Zhang, Q. Q., Zhang, X. Z., Hu, X. Y., Liu, E. Z., et al. (2020). Inter-plane heterojunctions within 2D/2D FeSe₂/g-C₃N₄ nanosheet semiconductors for photocatalytic hydrogen generation. *Appl. Catal. B Environ.* 261:118249. doi: 10.1016/j.apcatb.2019.118249
- Jiang, L. B., Yuan, X. Z., Pan, Y., Liang, J., Zeng, G. M., Wu, Z. B., et al. (2017). Doping of graphitic carbon nitride for photocatalysis: a review. *Appl. Catal. B Environ.* 217, 388–406. doi: 10.1016/j.apcatb.2017.06.003
- Lan, Z. A., Zhang, G., and Wang, X. (2016). A facile synthesis of Br-modified g-C₃N₄ semiconductors for photoredox water splitting. *Appl. Catal. B Environ.* 192, 116–125. doi: 10.1016/j.apcatb.2016.03.062
- Lee, A. H., Wang, Y. C., and Chen, C. C. (2019). Composite photocatalyst, tetragonal lead bismuth oxyiodide/bismuth oxyiodide/graphitic carbon nitride: Synthesis, characterization, photocatalytic activity. *J. Colloid Interf. Sci.* 533, 319–332. doi: 10.1016/j.jcis.2018.08.008
- Li, G. L., Guo, C. S., Yan, M., and Liu, S. Q. (2016). Cs_xWO₃ nanorods: realization of full-spectrum-responsive photocatalytic activities from UV, visible to near-infrared region. *Appl. Catal. B Environ.* 183, 142–148. doi: 10.1016/j.apcatb.2015.10.039
- Li, H. J., Qian, D. J., and Chen, M. (2015). Templateless infrared heating process for fabricating carbon nitride nanorods with efficient photocatalytic H₂ evolution. *ACS Appl. Mater. Inter.* 7, 25162–25170. doi: 10.1021/acsami.5b06627
- Li, J. Y., Cui, W., Sun, Y. J., Chu, Y. H., Cen, W. L., and Dong, F. (2017). Directional electron delivery via a vertical channel between g-C₃N₄ layers promotes photocatalytic efficiency. *J. Mater. Chem. A* 5, 9358–9364. doi: 10.1039/C7TA02183F
- Li, L. L., Bodedla, G. B., Liu, Z. T., and Zhu, X. J. (2020). Naphthalimide-porphyrin hybridized graphitic carbon nitride for enhanced photocatalytic hydrogen production. *Appl. Surf. Sci.* 499:143755. doi: 10.1016/j.apsusc.2019.143755
- Li, S. J., Chen, J. L., Hu, S. W., Wang, H. L., Jiang, W., and Chen, X. B. (2020). Facile construction of novel Bi₂WO₆/Ta₃N₅ Z-scheme heterojunction nanofibers for efficient degradation of harmful pharmaceutical pollutants. *Chem. Eng. J.* 402:126165. doi: 10.1016/j.cej.2020.126165
- Li, S. J., Hu, S. W., Jiang, W., Liu, Y., Zhou, Y. T., Liu, J. S., et al. (2018). Facile synthesis of cerium oxide nanoparticles decorated flower-like bismuth molybdate for enhanced photocatalytic activity toward organic pollutant degradation. *J. Colloid Interf. Sci.* 530, 171–178. doi: 10.1016/j.jcis.2018.06.084
- Li, S. J., Hu, S. W., Jiang, W., Zhang, J. L., Xu, K. B., and Wang, Z. H. (2019). In situ construction of WO₃ nanoparticles decorated Bi₂MoO₆ microspheres for boosting photocatalytic degradation of refractory pollutants. *J. Colloid Interf. Sci.* 556, 335–344. doi: 10.1016/j.jcis.2019.08.077
- Li, S. J., Xue, B., Chen, J. L., Liu, Y. P., Zhang, J. L., Wang, H. W., et al. (2021). Constructing a plasmonic p-n heterojunction photocatalyst of 3D Ag/Ag₆Si₂O₇/Bi₂MoO₆ for efficiently removing broad-spectrum antibiotics. *Sep. Purif. Technol.* 254:117579. doi: 10.1016/j.seppur.2020.117579
- Liang, Q. H., Li, Z., Huang, Z. H., Kang, F. Y., and Yang, Q. H. (2015). Holey graphitic carbon nitride nanosheets with carbon vacancies for highly improved photocatalytic hydrogen production. *Adv. Funct. Mater.* 25, 6885–6892. doi: 10.1002/adfm.201503221
- Liu, C. Y., Huang, H. W., Ye, L. Q., Yu, S. X., Tian, N., Du, X., et al. (2017). Intermediate-mediated strategy to horn-like hollow mesoporous ultrathin g-C₃N₄ tube with spatial anisotropic charge separation for superior photocatalytic H₂ evolution. *Nano Energy* 41, 738–748. doi: 10.1016/j.nanoen.2017.10.031
- Liu, G., Yan, S., Shi, L., and Yao, L. Z. (2019). The improvement of photocatalysis H₂ evolution over g-C₃N₄ with Na and cyano-group co-modification. *Front. Chem.* 7, 639–645. doi: 10.3389/fchem.2019.00639
- Liu, L., Luo, X., Li, Y. Z., Xu, F., Gao, Z. B., Zhang, X. N., et al. (2018). Facile synthesis of few-layer g-C₃N₄/ZnO composite photocatalyst for enhancing visible light photocatalytic performance of pollutants removal. *Colloid. Surf. A* 537, 516–523. doi: 10.1016/j.colsurfa.2017.09.051
- Liu, M. J., Wageh, S., Al-Ghamdi, A. A., Xia, P. F., Cheng, B., Zhang, L. Y., et al. (2019). Quenching induced hierarchical 3D porous g-C₃N₄ with enhanced photocatalytic CO₂ reduction activity. *Chem. Commun.* 55, 14023–14026. doi: 10.1039/C9CC07647F

- Liu, Q., Chen, T. X., Guo, Y. R., Zhang, Z. G., and Fang, X. M. (2016). Ultrathin g-C₃N₄ nanosheets coupled with carbon nanodots as 2D/0D composites for efficient photocatalytic H₂ evolution. *Appl. Catal. B Environ.* 193, 248–258. doi: 10.1016/j.apcatb.2016.04.034
- Liu, Q. W., Wang, J. M., Liu, D., Li, R. J., and Peng, T. Y. (2018). Photosensitization of zinc phthalocyanine bearing 15-crown-5 ether moieties on carbon nitride for H₂ production: Effect of co-existing alkali metal ions. *J. Power Sources* 396, 57–63. doi: 10.1016/j.jpowsour.2018.05.098
- Liu, S. Z., Sun, H. Q., Ang, H. M., Tade, M. O., and Wang, S. (2016). Integrated oxygen-doping and dye sensitization of graphitic carbon nitride for enhanced visible light photodegradation. *J. Colloid Interf. Sci.* 476, 193–199. doi: 10.1016/j.jcis.2016.05.026
- Liu, X. C., Liu, L., Yao, Z. R., Yang, Z. H., and Xu, H. (2020). Enhanced visible-light-driven photocatalytic hydrogen evolution and NO photo-oxidation capacity of ZnO/g-C₃N₄ with N dopant. *Colloid. Surf. A* 599:124869. doi: 10.1016/j.colsurfa.2020.124869
- Liu, Y. F., He, M. F., Guo, R., Fang, Z. R., Kang, S. F., Z., et al. (2020a). Ultrastable metal-free near-infrared-driven photocatalysts for H₂ production based on protonated 2D g-C₃N₄ sensitized with Chlorin e6. *Appl. Catal. B Environ.* 260:118137. doi: 10.1016/j.apcatb.2019.118137
- Liu, Y. F., Kang, S. F., Cui, L. F., and Ma, Z. (2020b). Boosting near-infrared-driven photocatalytic H₂ evolution using protoporphyrin-sensitized g-C₃N₄. *J. Photochem. Photobiol. A* 396:112517. doi: 10.1016/j.jphotochem.2020.112517
- Liu, Y. Z., Zhang, H. Y., Ke, J., Zhang, J. Q., Tian, W. J., Xu, X. Y., et al. (2018). 0D (MoS₂)/2D (g-C₃N₄) heterojunctions in Z-scheme for enhanced photocatalytic and electrochemical hydrogen evolution. *Appl. Catal. B Environ.* 228, 64–74. doi: 10.1016/j.apcatb.2018.01.067
- Luo, B., Song, R., Geng, J. F., Jing, D. W., and Zhang, Y. Z. (2018). Facile preparation with high yield of a 3D porous graphitic carbon nitride for dramatically enhanced photocatalytic H₂ evolution under visible light. *Appl. Catal. B Environ.* 238, 294–301. doi: 10.1016/j.apcatb.2018.07.039
- Mamba, G., and Mishra, A. K. (2016). Graphitic carbon nitride (g-C₃N₄) nanocomposites: a new and exciting generation of visible light driven photocatalysts for environmental pollution remediation. *Appl. Catal. B Environ.* 198, 347–377. doi: 10.1016/j.apcatb.2016.05.052
- Marangon, I., Ménard-Moyon, C., Silva, A. K. A., Bianco, A., Luciani, N., and Gazeau, F. (2016). Synergic mechanisms of photothermal and photodynamic therapies mediated by photosensitizer/carbon nanotube complexes. *Carbon* 97, 110–123. doi: 10.1016/j.carbon.2015.08.023
- Mishra, A., Mehta, A., Basu, S., Shetti, N. P., Reddy, K. R., and Aminabhavi, T. M. (2019). Graphitic carbon nitride (g-C₃N₄)-based metal-free photocatalysts for water splitting: a review. *Carbon* 149, 693–721. doi: 10.1016/j.carbon.2019.04.104
- Murugesan, P., Moses, J. A., and Anandharamkrishnan, C. (2019). Photocatalytic disinfection efficiency of 2D structure graphitic carbon nitride-based nanocomposites: a review. *J. Mater. Sci.* 54, 12206–12235. doi: 10.1007/s10853-019-03695-2
- Naseri, A., Samadi, M., Pourjavadi, A., Moshfegh, A. Z., and Ramakrishna, S. (2017). Graphitic carbon nitride (g-C₃N₄)-based photocatalysts for solar hydrogen generation: recent advances and future development directions. *J. Mater. Chem. A* 5, 23406–23433. doi: 10.1039/C7TA05131J
- Navarro, F. P., Creusat, G., Frochot, C., Moussaron, A., Verhille, M., Vandresse, R., et al. (2014). Preparation and characterization of mTHPC-loaded solid lipid nanoparticles for photodynamic therapy. *J. Photochem. Photobiol. B Biol.* 130, 161–169. doi: 10.1016/j.jphotobiol.2013.11.007
- Ong, W. J., Putri, L. K., Tan, Y. C., Tan, L. L., Li, N., Ng, Y. H., et al. (2017). Unravelling charge carrier dynamics in protonated g-C₃N₄ interfaced with carbon nanodots as co-catalysts toward enhanced photocatalytic CO₂ reduction: a combined experimental and first-principles DFT study. *Nano Res.* 10, 1673–1696. doi: 10.1007/s12274-016-1391-4
- Ouedraogo, S., Chouchene, B., Desmarests, C., Gries, T., Balan, L., Fournet, R., et al. (2018). Copper octacarbonylphthalocyanine as sensitizer of graphitic carbon nitride for efficient dye degradation under visible light irradiation. *Appl. Catal. A Gen.* 563, 127–136. doi: 10.1016/j.apcata.2018.06.036
- Pan, Z. M., Zheng, Y., Guo, F. S., Niu, P. P., and Wang, X. C. (2017). Decorating CoP and Pt nanoparticles on graphitic carbon nitride nanosheets to promote overall water splitting by conjugated polymers. *ChemSusChem* 10, 87–90. doi: 10.1002/cssc.201600850
- Pannari, S., Ganguly, P., Nair, B. N., Mohamed, A. A. P., Warrier, K. G. K., and Hareesh, U.N.S. (2017). Role of precursors on the photophysical properties of carbon nitride and its application for antibiotic degradation. *Environ. Sci. Pollut. Control. Ser. 24*, 8609–8618. doi: 10.1007/s11356-017-8538-z
- Prabavathi, S., and Muthuraj, V. (2019). Superior visible light driven photocatalytic degradation of fluoroquinolone drug norfloxacin over novel NiWO₄ nanorods anchored on g-C₃N₄ nanosheets. *Colloid. Surf. A* 567, 43–54. doi: 10.1016/j.colsurfa.2019.01.040
- Qi, K. Z., Li, Y., Xie, Y. B., Liu, S. Y., Zheng, K., Chen, Z., et al. (2019). Ag loading enhanced photocatalytic activity of g-C₃N₄ porous nanosheets for decomposition of organic pollutants. *Front. Chem.* 7, 91–100. doi: 10.3389/fchem.2019.00091
- Qin, J. Y., and Zeng, H. P. (2017). Photocatalysts fabricated by depositing plasmonic Ag nanoparticles on carbon quantum dots/graphitic carbon nitride for broad spectrum photocatalytic hydrogen generation. *Appl. Catal. B Environ.* 209, 161–173. doi: 10.1016/j.apcatb.2017.03.005
- Qiu, L. F., Qiu, X. B., Li, P., Ma, M. F., Chen, X. S., and Duo, S. W. (2020). *In-situ* self-assembly synthesis of 2D/2D CdS/g-C₃N₄ heterojunction for efficient visible-light photocatalytic performance. *Mater. Lett.* 268:127566. doi: 10.1016/j.matlet.2020.127566
- Qiu, P. X., Xu, C. M., Chen, H. Q., Jiang, F., Wang, X., Lu, R. F., et al. (2017). One step synthesis of oxygen doped porous graphitic carbon nitride with remarkable improvement of photo-oxidation activity: role of oxygen on visible light photocatalytic activity. *Appl. Catal. B Environ.* 206, 319–327. doi: 10.1016/j.apcatb.2017.01.058
- Ran, J., Ma, T. Y., Gao, G., Du, X. W., and S. Z., Qiao, C.B. (2015). Porous P-doped graphitic carbon nitride nanosheets for synergistically enhanced visible-light photocatalytic H₂ production. *Energy Environ. Sci.* 8, 3708–3717. doi: 10.1039/C5EE02650D
- She, X. J., Liu, L., Ji, H. Y., Mo, Z., Li, Y. P., Huang, L. Y., et al. (2016). Template-free synthesis of 2D porous ultrathin nonmetal-doped g-C₃N₄ nanosheets with highly efficient photocatalytic H₂ evolution from water under visible light. *Appl. Catal. B Environ.* 187, 144–153. doi: 10.1016/j.apcatb.2015.12.046
- Shen, X. F., Yang, J. Y., Zheng, T., Wang, Q., Zhuang, H. F., Zheng, R. N., et al. (2020a). Plasmonic p-n heterojunction of Ag/Ag₂S/Ag₂MoO₄ with enhanced Vis-NIR photocatalytic activity for purifying wastewater. *Sep. Purif. Technol.* 251:117347. doi: 10.1016/j.seppur.2020.117347
- Shen, X. F., Zhang, T. Y., Xu, P. F., Zhang, L. S., Liu, J. S., and Chen, Z. G. (2017). Growth of C₃N₄ nanosheets on carbon-fiber cloth as flexible and macroscale filter-membrane-shaped photocatalyst for degrading the flowing wastewater. *Appl. Catal. B Environ.* 219, 425–431. doi: 10.1016/j.apcatb.2017.07.059
- Shen, X. F., Zheng, T., Yang, J. Y., Shi, Z., Xue, Q. Q., Liu, W. P., et al. (2020b). Removal of Cr(VI) from acid wastewater by BC/ZnFe₂O₄ magnetic nanocomposite via the synergy of absorption-photocatalysis. *ChemCatChem* 12, 4121–4131. doi: 10.1002/cctc.202000619
- Shi, W. L., Li, M. Y., Huang, X. L., Ren, H. J., Yan, C., and Guo, F. (2020). Facile synthesis of 2D/2D Co₃(PO₄)₂/g-C₃N₄ heterojunction for highly photocatalytic overall water splitting under visible light. *Chem. Eng. J.* 382:122960. doi: 10.1016/j.cej.2019.122960
- Shiraishi, Y., Kofuji, Y., Kanazawa, S., Sakamoto, H., Ichikawa, S., Tanaka, S., et al. (2014). Platinum nanoparticles strongly associated with graphitic carbon nitride as efficient co-catalysts for photocatalytic hydrogen evolution under visible light. *Chem. Commun.* 50, 15255–15258. doi: 10.1039/C4CC06960A
- Sui, Y., Liu, J. H., Zhang, Y. W., Tian, X. K., and Chen, W. (2013). Dispersed conductive polymer nanoparticles on graphitic carbon nitride for enhanced solar-driven hydrogen evolution from pure water. *Nanoscale* 5, 9150–9155. doi: 10.1039/c3nr02413j
- Sun, S. D., and Liang, S. H. (2017). Recent advances in functional mesoporous graphitic carbon nitride (mpg-C₃N₄) polymers. *Nanoscale* 9, 10544–10578. doi: 10.1039/C7NR03656F
- Sun, X. Y., Zhang, F. J., Kong, C. (2020). Porous g-C₃N₄/WO₃ photocatalyst prepared by simple calcination for efficient hydrogen generation under visible light. *Colloid. Surf. A* 594:124653. doi: 10.1016/j.colsurfa.2020.124653
- Tao, W., Wang, M. K., Ali, R., Nie, S., Zeng, Q. L., Yang, R. Q., et al. (2019). Multi-layered porous hierarchical TiO₂/g-C₃N₄ hybrid coating for enhanced visible light photocatalysis. *Appl. Surf. Sci.* 495:143435. doi: 10.1016/j.apsusc.2019.07.177

- Teng, Z. Y., Lv, H. Y., Wang, C. Y., Xue, H. G., Pang, H., and Wang, G. X. (2017). Bandgap engineering of ultrathin graphene-like carbon nitride nanosheets with controllable oxygenous functionalization. *Carbon* 113, 63–75. doi: 10.1016/j.carbon.2016.11.030
- Tian, N., Zhang, Y. H., Li, X. W., Xiao, K., Du, X., Dong, F., et al. (2017). Precursor-reforming protocol to 3D mesoporous g-C₃N₄ established by ultrathin self-doped nanosheets for superior hydrogen evolution. *Nano Energy* 38, 72–81. doi: 10.1016/j.nanoen.2017.05.038
- Tian, S. F., Chen, S. D., Ren, X. T., Cao, R. H., Hu, H. Y., and Bai, F. (2019). Bottom-up fabrication of graphitic carbon nitride nanosheets modified with porphyrin via covalent bonding for photocatalytic H₂ evolution. *Nano Res.* 12, 3109–3115. doi: 10.1007/s12274-019-2562-x
- Wang, D. H., Pan, J. N., Li, H. H., Liu, J. J., Wang, Y. B., Kang, L. T., et al. (2016). A pure organic heterostructure of μ -oxo dimeric iron(III) porphyrin and graphitic-C₃N₄ for solar H₂ reduction from water. *J Mater Chem A* 4, 290–296. doi: 10.1039/C5TA07278F
- Wang, F. L., Wang, Y. F., Feng, Y. P., Zeng, Y. Q., Xie, Z. J., Zhang, Q. X., et al. (2018). Novel ternary photocatalyst of single atom-dispersed silver and carbon quantum dots co-loaded with ultrathin g-C₃N₄ for broad spectrum photocatalytic degradation of naproxen. *Appl. Catal. B Environ.* 221, 510–520. doi: 10.1016/j.apcatb.2017.09.055
- Wang, K., Li, Y., Li, J., and Zhang, G. K. (2020). Boosting interfacial charge separation of Ba₅Nb₄O₁₅/g-C₃N₄ photocatalysts by 2D/2D nanojunction towards efficient visible-light driven H₂ generation. *Appl. Catal. B Environ.* 263:117730. doi: 10.1016/j.apcatb.2019.05.032
- Wang, N., Han, B., Wen, J. B., Liu, M. W., and Li, X. J. (2019). Synthesis of novel Mn-doped Fe₂O₃ nanocube supported g-C₃N₄ photocatalyst for overall visible-light driven water splitting. *Colloid. Surf. A* 567, 313–318. doi: 10.1016/j.colsurfa.2019.01.053
- Wang, X. C., Maeda, K., Thomas, A., Takanabe, K., Xin, G., Carlsson, J. M., et al. (2009). A metal-free polymeric photocatalyst for hydrogen production from water under visible light. *Nat. Mater.* 8, 76–80. doi: 10.1038/nmat2317
- Wang, Z. Y., Huang, Y., Ho, W. K., Cao, J. J., Shen, Z. X., and Lee, S. C. (2016). Fabrication of Bi₂O₂CO₃/g-C₃N₄ heterojunctions for efficiently photocatalytic NO in air removal: *in-situ* self-sacrificial synthesis, characterizations and mechanistic study. *Appl. Catal. B Environ.* 199, 123–133. doi: 10.1016/j.apcatb.2016.06.027
- Wei, F., Liu, Y., Zhao, H., Ren, X., Liu, J., Hasan, T., et al. (2018). Oxygen self-doped g-C₃N₄ with tunable electronic band structure for unprecedentedly enhanced photocatalytic performance. *Nanoscale* 10, 4515–4522. doi: 10.1039/C7NR09660G
- Wennink, J. W. H., Liu, Y. N., Makinen, P. I., Setaro, F., Escosura, A., Bourajjaj, M., et al. (2017). Macrophage selective photodynamic therapy by meta-tetra(hydroxyphenyl)chlorin loaded polymeric micelles: a possible treatment for cardiovascular diseases. *Eur. J. Pharm. Sci.* 107, 112–125. doi: 10.1016/j.ejps.2017.06.038
- Xiao, X., Wang, Y. H., Bo, Q., Xu, X. Y., and Zhang, D. G. (2020). One-step preparation of sulfur-doped porous g-C₃N₄ for enhanced visible light photocatalytic performance. *Dalton Trans.* 49, 8041–8050. doi: 10.1039/D0DT00299B
- Xie, L. F., Ni, J., Tang, B., He, G. Y., and Chen, H. Q. (2018). A self-assembled 2D/2D-type protonated carbon nitride-modified graphene oxide nanocomposite with improved photocatalytic activity. *Appl. Surf. Sci.* 434, 456–463. doi: 10.1016/j.apsusc.2017.10.193
- Xing, Z., Chen, Z. G., Zong, X., and L., Wang, Z. (2014). A new type of carbon nitride-based polymer composite for enhanced photocatalytic hydrogen production. *Chem. Commun.* 50, 6762–6764. doi: 10.1039/C4CC00397G
- Yang, Y. J., Sun, B. W., Qian, D. J., and Chen, M. (2019). Fabrication of multiporphyrin@g-C₃N₄ nanocomposites via Pd(II)-directed layer-by-layer assembly for enhanced visible-light photocatalytic activity. *Appl. Surf. Sci.* 478, 1027–1036. doi: 10.1016/j.apsusc.2019.02.028
- Ye, R. Q., Fang, H. B., Zheng, Y. Z., Li, N., Wang, Y., and Tao, X. (2016). Fabrication of CoTiO₃/g-C₃N₄ hybrid photocatalysts with enhanced H₂ evolution: Z-scheme photocatalytic mechanism insight. *ACS Appl. Mater. Interfaces* 8, 13879–13889. doi: 10.1021/acsami.6b01850
- Yu, H. J., Shi, R., Zhao, Y. X., Bian, T., Zhao, Y. F., Zhou, C., et al. (2017). Alkali-assisted synthesis of nitrogen deficient graphitic carbon nitride with tunable band structures for efficient visible-light-driven hydrogen evolution. *Adv. Mater.* 29:1605148. doi: 10.1002/adma.201605148
- Yuan, Y. J., Lu, H. W., Ji, Z. G., Zhong, J. S., Ding, M. Y., Chen, D. Q., et al. (2015a). Enhanced visible-light-induced hydrogen evolution from water in a noble-metal-free system catalyzed by ZnTCPP-MoS₂/TiO₂ assembly. *Chem. Eng. J* 275, 8–16. doi: 10.1016/j.cej.2015.04.015
- Yuan, Y. J., Shen, Z. K., Wang, P., Li, Z. J., Pei, L., Zhong, J. S., et al. (2020). Metal-free broad-spectrum PTCDA/g-C₃N₄ Z-scheme photocatalysts for enhanced photocatalytic water oxidation. *Appl. Catal. B Environ.* 260:118179. doi: 10.1016/j.apcatb.2019.118179
- Yuan, Y. J., Tu, J. R., Ye, Z. J., Lu, H. W., Ji, Z. G., Hu, B., et al. (2015b). Visible-light-driven hydrogen production from water in a noble-metal-free system catalyzed by zinc porphyrin sensitized MoS₂/ZnO. *Dyes Pigments* 123, 285–292. doi: 10.1016/j.dyepig.2015.08.014
- Zada, A., Khan, M., Qureshi, M. N., Liu, S. Y., and Wang, R. D. (2019). Accelerating photocatalytic hydrogen production and pollutant degradation by functionalizing g-C₃N₄ with SnO₂. *Front. Chem.* 7, 941–949. doi: 10.3389/fchem.2019.00941
- Zeng, P., Wang, J. M., Guo, Y. Y., Li, R. J., Mei, G. Q., and Peng, T. Y. (2019). Synthesis of an A₂BC-type asymmetric zinc phthalocyanine derivative for efficient visible/near-infrared-driven H₂ evolution on g-C₃N₄. *Chem. Eng. J.* 373, 651–659. doi: 10.1016/j.cej.2019.05.073
- Zeng, Y. X., Liu, C. B., Wang, L. L., Zhang, S. Q., Ding, Y. B., Xu, Y. Z., et al. (2016). A three-dimensional graphitic carbon nitride belt network for enhanced visible light photocatalytic hydrogen evolution. *J. Mater. Chem. A* 4, 19003–19010. doi: 10.1039/C6TA07397B
- Zhang, G., Lan, Z. A., and Wang, X. (2017). Surface engineering of graphitic carbon nitride polymers with cocatalysts for photocatalytic overall water splitting. *Chem. Sci.* 8, 5261–5274. doi: 10.1039/C7SC01747B
- Zhang, J. L., and Ma, Z. (2017a). Ag₆Mo₁₀O₃₃/g-C₃N₄ 1D-2D hybridized heterojunction as an efficient visible-light-driven photocatalyst. *Mol. Catal.* 432, 285–291. doi: 10.1016/j.mcat.2017.02.024
- Zhang, J. L., and Ma, Z. (2017b). Novel β -Ag₂MoO₄/g-C₃N₄ heterojunction catalysts with highly enhanced visible-light-driven photocatalytic activity. *RSC Adv.* 7, 2163–2171. doi: 10.1039/C6RA26352F
- Zhang, J. S., Chen, X. F., Takanabe, K., Maeda, K., Domen, K., Epping, J. D., et al. (2010). Synthesis of a carbon nitride structure for visible-light catalysis by copolymerization. *Angew. Chem. Int. Ed.* 49, 441–444. doi: 10.1002/anie.200903886
- Zhang, J. S., Chen, Y., and Wang, X. C. (2015). Two-dimensional covalent carbon nitride nanosheets: synthesis, functionalization, and applications. *Energy Environ. Sci.* 8, 3092–3108. doi: 10.1039/C5EE01895A
- Zhang, X. H., Lin, L., Qu, D., Yang, J. G., Weng, Y. X., Wang, Z., et al. (2020). Boosting visible-light driven solar-fuel production over g-C₃N₄/tetra(4-carboxyphenyl)porphyrin iron(III) chloride hybrid photocatalyst via incorporation with carbon dots. *Appl. Catal. B Environ.* 265:118595. doi: 10.1016/j.apcatb.2020.118595
- Zhang, X. H., Peng, T. Y., Yu, L. J., Li, R. J., Li, Q. Q., and Li, Z. (2015). Visible/near-infrared-light-induced H₂ production over g-C₃N₄ co-sensitized by organic dye and zinc phthalocyanine derivative. *ACS Catal.* 5, 504–510. doi: 10.1021/cs5016468
- Zhang, X. H., Yu, L. J., Zhuang, C. S., Peng, T. Y., Li, R. J., and Li, X. G. (2014). Highly asymmetric phthalocyanine as a sensitizer of graphitic carbon nitride for extremely efficient photocatalytic H₂ production under near-infrared light. *ACS Catal.* 4, 162–170. doi: 10.1021/cs400863c
- Zhao, Z. W., Sun, Y. J., Dong, F., Zhang, Y. X., and Zhao, H. (2015). Template synthesis of carbon self-doped g-C₃N₄ with enhanced visible to near-infrared absorption and photocatalytic performance. *RSC Adv.* 5, 39549–39556. doi: 10.1039/C5RA03433G

- Zheng, Y., Lin, L. H., Wang, B., and Wang, X. C. (2015). Graphitic carbon nitride polymers toward sustainable photoredox catalysis. *Angew. Chem. Int. Ed.* 54, 12868–12884. doi: 10.1002/anie.201501788
- Zhou, X. B., Li, Y. F., Xing, Y., Li, J. S., and Jiang, X. (2019). Effects of the preparation method of Pt/g-C₃N₄ photocatalysts on their efficiency for visible-light hydrogen production. *Dalton Trans.* 48, 15068–15073. doi: 10.1039/C9DT02938A
- Zou, J. P., Wang, L. C., Luo, J., Nie, Y. C., Xing, Q. J., Luo, X. B., et al. (2016). Synthesis and efficient visible light photocatalytic H₂ evolution of a metal-free g-C₃N₄/graphene quantum dots hybrid photocatalyst. *Appl. Catal. B. Environ.* 193, 103–109. doi: 10.1016/j.apcatb.2016.04.017

Conflict of Interest: The authors declare that the research was conducted in the absence of any commercial or financial relationships that could be construed as a potential conflict of interest.

Copyright © 2020 Liu and Ma. This is an open-access article distributed under the terms of the Creative Commons Attribution License (CC BY). The use, distribution or reproduction in other forums is permitted, provided the original author(s) and the copyright owner(s) are credited and that the original publication in this journal is cited, in accordance with accepted academic practice. No use, distribution or reproduction is permitted which does not comply with these terms.